NASA Technical Memorandum 81302

USAAVRADCOM TR 81-B-16

The Influence of Unsteady Aerodynamics on Hingeless Rotor Ground Resonance

Wayne Johnson

July 1981

National Aeronautics and Space Administration

United States Army Aviation Research and Development Command

NASA Technical Memorandum 81302

USAAVRADCOM TR 81-B-16

The Influence of Unsteady Aerodynamics on Hingeless Rotor Ground Resonance

Wayne Johnson, Aeromechanics Laboratory
AVRADCOM Research and Technology Laboratories
Ames Research Center, Moffett Field, California

NASA
National Aeronautics and Space Administration
Ames Research Center
Moffett Field, California 94035

United States Army Aviation Research and Development Command

THE INFLUENCE OF UNSTEADY AERODYNAMICS ON HINGELESS ROTOR GROUND RESONANCE

Wayne Johnson

Ames Research Center

and

Aeromechanics Laboratory

AVRADCOM Research and Technology Laboratories

SUMMARY

Calculations of the modal frequency and damping for a hingeless rotor on a gimballed support in hover are compared with measured results for two configurations (differing in blade flap stiffness). Good correlation is obtained when an inflow dynamics model is used to account for the influence of the unsteady aerodynamics. The effect of the unsteady aerodynamics is significant for this rotor system. The inflow dynamics model introduces additional states corresponding to perturbations of the wake induced velocity at the rotor disk. The calculations confirm the experimental observation that the inflow mode introduced by these additional states is measureable for one configuration but not for the other.

NOMENCLATURE

C	lift deficiency function
M	body pitch moment
s	eigenvalue, $s = \sigma \pm i\omega$
β_p	progressing (high frequency) flap mode
β_r	regressing (low frequency) flap mode
ζ	damping ratio, $\zeta = -\mathrm{Re}\, s/\lvert s \rvert$
ζ_p	progressing (high frequency) lag mode
ζ_r	regressing (low frequency) lag mode
θ	body pitch mode; body pitch degree of freedom
κ	factor in time lag of inflow
λ	inflow mode
λ_0	inflow ratio: mean induced velocity of rotor, divided by tip speed
λ_x	longitudinal induced velocity perturbation
λ_y	lateral induced velocity perturbation
σ	modal damping, $\sigma = \mathrm{Re}\, s$
ϕ	body roll mode; body roll degree of freedom
ω	modal frequency, $\omega = \mathrm{Im}\, s$; system excitation frequency
Ω	rotor rotational speed

INTRODUCTION

The importance of unsteady aerodynamic forces in aeroelastic phenomena has long been acknowledged, based on both fixed wing and rotary wing experience. Yet an entirely satisfactory model for the unsteady aerodynamics of a helicopter rotor is still not available, particularly for problems such as flutter stability and handling qualities that involve transient motion of the system. A model for the noncirculatory loads can be readily obtained from two-dimensional unsteady airfoil theory, but the results from either two-dimensional or fixed-wing three-dimensional wing theory for the circulatory loads are not applicable since the wake models are not correct for rotary wings. The development of a general theory for rotary wing unsteady airloads is difficult due to the complex geometry of the rotor wake, even in hover. Moreover, in forward flight a time-invariant model of the system is not possible due to the periodically varying aerodynamic environment of the blades. Consequently attention has recently been focused on the development of relatively simple models for the unsteady aerodynamics. These models take the form of differential equations for parameters defining the wake-induced velocity distribution at the rotor disk.

The development of such an inflow dynamics model involves two steps. The first step is the identification, from analysis or experiment, of the structure and parameters of the unsteady aerodynamics model. The second step is the verification of the model by correlation of calculations and measurements for progressively more diverse and complex aeroelastic

problems. Considerable progress has been made with the first step, although much remains to be done. The present paper is a contribution to the second step. Bousman (Ref. 1) has produced a set of experimental data that provides an opportunity to examine the influence of inflow dynamics on the coupled behavior of a rotor and body. In the sections below, the inflow dynamics model used and the experimental system will be described. Then the measured data will be compared to calculations obtained with and without the inflow dynamics model, and the influence of unsteady aerodynamics on this system will be discussed.

PERTURBATION INFLOW MODEL FOR ROTOR UNSTEADY AERODYNAMICS

The inflow dynamics model used here is derived in detail in Refs. 2 and 3. For the present purposes only the inflow perturbation due to pitch and roll moments in hover is considered. A wake-induced velocity perturbation that varies linearly over the rotor disk is defined by

$$\delta\lambda = \lambda_x r\cos\Psi + \lambda_y r\sin\Psi$$

where r and Ψ are the polar coordinates of the disk. The variables λ_x and λ_y are related to the aerodynamic pitch and roll moment coefficients (C_{M_y} and C_{M_x}) by first order differential equations:

$$\tau\begin{pmatrix}\lambda_x\\ \lambda_y\end{pmatrix}^{\bullet} + \begin{pmatrix}\lambda_x\\ \lambda_y\end{pmatrix} = \frac{\partial\lambda}{\partial M}\begin{pmatrix}-C_{M_y}\\ C_{M_x}\end{pmatrix}_{aero}$$

where $\tau = k(\partial\lambda/\partial M)$, with k a constant.

The factor $\partial\lambda/\partial M$ can be obtained from differential momentum theory as follows (Ref. 2). A thrust perturbation dT on the element of

disk area dA is related to the inflow perturbation by $dT = \dot{m}\, 2\, \delta v$, where the mass flow rate is $\dot{m} = \rho v_0\, dA$ (v_0 and δv are the mean and perturbation inflow velocities, written λ_0 and $\delta\lambda$ when made dimensionless by dividing by the rotor tip speed). Hence

$$\delta v = \frac{dT/dA}{2\rho v_0}$$

A linear variation of δv over the rotor disk implies a linear variation of the loading dT/dA, which corresponds to pitch and roll moments. Integration of this expression over the rotor disk produces then $\partial\lambda/\partial M = 2/\lambda_0$. This result for $\partial\lambda/\partial M$ can be derived more rigorously by means of unsteady actuator disk theory (Refs. 2, 4, and 5). Neglecting the time lag, the factor $\partial\lambda/\partial M = 2/\lambda_0$ produces a lift deficiency function of

$$C = \frac{1}{1 + \frac{\sigma a}{\rho \lambda_0}}$$

(see Ref. 2; here a is the blade section lift curve slope and σ is the rotor solidity ratio), which is identical to the low frequency approximation to Loewy's lift deficiency function for harmonic loading (Ref. 2):

$$C = \frac{1}{1 + \frac{\pi}{h/b}}$$

(where h/b is the ratio of the shed wake vertical spacing to the blade semichord, hence $h/b = 4\lambda_0/\sigma$). The result $\partial\lambda/\partial M = 2/\lambda_0$ for moment perturbations in hover is also supported by parameter identification from measurements of rotor flap response to cyclic control (Refs. 6 and 7).

The parameter k in the inflow time lag is obtained by considering the apparent mass of an impermeable disk subject to an angular

acceleration (Ref. 8):

$$k = \frac{16}{45\pi} = 0.113$$

This value is supported by comparison with experimental data (Ref. 9, for thrust perturbations) and by parameter identification results (Refs. 5 and 7). The value of k seems to depend on the rotor mean loading distribution (Ref. 5). There is some indication that a larger value (.226, Ref. 10) or smaller value (.086, Ref. 5) is appropriate in certain cases. Without the time lag ($k = 0$), a quasistatic inflow model is obtained, the effects of which are expressed by the lift deficiency function λ given above. For rotor dynamics problems in which the dominant aerodynamic forces are the lift perturbations due to angle of attack changes, the magnitude of the aerodynamic influence is described by the blade Lock number (which contains the section lift curve slope). Hence in such cases the effects of the quasistatic inflow model can be largely represented by the use of an effective Lock number that is the product of the actual Lock number and the lift deficiency function (Refs. 11 and 12). A quasistatic inflow dynamics model has long been used in handling qualities analyses (see Ref. 13 for example). A very large value of the time lag ($k \to \infty$) would eliminate the influence of the inflow dynamics.

Experimental measurements of hub moment response to cyclic control and shaft oscillations show a significant influence of the inflow dynamics (Ref. 8). The role of the inflow dynamics was identified in these measurements by correlation with calculations using the above model; the good correlation obtained provides further support for the values of $\partial\lambda/\partial M$ and k. Calculations

of flap-lag stability also predict a significant influence of the inflow dynamics (Refs. 14 and 15). The need for the time lag appears to depend on the problem involved. The influence of the time lag is often enough to be measureable, but the quasistatic model may still give qualitatively correct results. The inflow dynamics model is not quite as well developed for forward flight as for hover, but considerable progress has been made (see Refs. 5, 8, 12, 14-16).

DESCRIPTION OF THE EXPERIMENTAL APPARATUS

The experimental data considered here were obtained in an investigation of ground resonance stability in hover (Ref 1). A model rotor with hingeless blades, on a gimbal support with pitch and roll degrees of freedom was tested. The primary parameters describing the system are given in Table 1. The experimental apparatus and test techniques are described in detail in Ref. 1. Most of the results presented in this paper are for a collective pitch of zero, but the cambered airfoil used has zero lift at an angle of attack of -1.5°. Hence the rotor had a small positive thrust value at zero collective pitch. A lift curve slope of 6.59 was used for this airfoil at low Reynolds number. The blades had flap and lag flexures at radial station 0.105R, with no pitch/flap or pitch/lag couplings. The collective pitch was introduced outboard of the flexures. The blades were very stiff in torsion. Two flap flexures were used: configuration 1, for which the flap flexure had one-fourth the stiffness of the lag flexure; and configuration 4, with equal flap and lag flexure stiffnesses. (The designation "configuration 4" follows Ref. 1.)

Table 1. Rotor Parameters

Number of blades	3
Radius, R	0.911 m
Solidity ratio	0.0494
Lock number	8.4
Twist	0
Tip Mach number (at 1000 rpm)	0.25
Tip Reynolds number (at 1000 rpm)	243000.
Airfoil	NACA 23012
Height hub above gimbal	0.241 m
Nonrotating lag frequency	
Configuration 1	6.70 Hz
Configuration 4	6.73 Hz
Nonrotating flap frequency	
Configuration 1	3.13 Hz
Configuration 4	6.63 Hz

The blade lag stiffness was such that the rotating natural frequency of the lag mode was below once-per-revolution for rotor speeds above 445 rpm. The springs on the gimbal produced resonances between the regressing lag mode and the body pitch and roll modes at rotor speeds of about 595 rpm and 765 rpm respectively (see Table 2). At such resonance, with the blade lag frequency below 1/rev, a ground resonance instability is possible if the system damping is low enough (Ref. 2).

DESCRIPTION OF THE ANALYSIS

The aeroelastic stability of this system was calculated using the analysis described in Ref. 3. The only rotor degrees of freedom considered were the fundamental flap and lag modes of each of the three blades. The body degrees of freedom consisted of pitch and roll motion about the gimbal. In hover, the coning and collective lag modes do not couple with such body motion. Hence the analytical model consisted of the rotor cyclic flap, cyclic lag, and body pitch and roll degrees of freedom (12 states). The variables λ_x and λ_y were included when the inflow dynamics model was used (14 states). The parameters required by the analysis were determined from the known values of the geometry, inertias, nonrotating frequencies, and nonrotating damping of the rotor and body (Ref. 1).

RESULTS FOR CONFIGURATION 1

In Figs. 1 to 5 the measured modal frequencies and damping for configuration 1 (the soft flap flexure) are a function of rotor speed are compared with calculations. The collective pitch is zero. The calculated

Table 2. Rotor-Body Resonances

	Configuration 1	Configuration 4
Pitch mode		
Rotor speed (rpm)	595	605
Flap frequency (per rev)	1.14	1.27
Lag frequency (per rev)	0.81	0.79
Roll mode		
Rotor speed (rpm)	745	780
Flap frequency (per rev)	1.12	1.20
Lag frequency (per rev)	0.69	0.67

results are for two cases: with and without the inflow dynamics model. The modal frequencies ω are shown in Figs. 1 and 2, and the damping σ of the regressing lag, body pitch, and body roll modes is shown in Figs. 3 to 5. The eigenvalue is $s = \sigma \pm i\omega$; a mode is unstable if σ is positive. The regressing lag mode damping shows a ground resonance instability due to coupling with the roll mode. The designation of the modes in these and the succeeding figures is defined in the nomenclature list. Without the inflow dynamics model, the calculated frequencies of the body modes are too low for rotor speeds above the resonances (Fig. 2); the lag mode is too stable at the resonance (Fig. 3); the pitch mode damping is too high (Fig. 4); and the roll mode damping is far too high (Fig. 5). The body structural damping is small (note the value at $\Omega = 0$), so the discrepancies in Figs. 4 and 5 are due to the aerodynamic forces. With the inflow dynamics model, the frequencies are predicted well (Fig. 1); the calculation of the lag mode damping is improved, although it is still too stable at the resonance (Fig. 3); the pitch mode damping is predicted well, except that it is somewhat low at high rotor speed (Fig. 4); and the calculated roll mode damping correlates well with the measurements (Fig. 5). The prediction of the lag mode damping at the ground resonance instability could be improved by reducing the structural damping of the rotor lag or body roll motion -- if some rational approach for making such a change could be established. Note that there are significant shifts in the body frequencies at low rotor speed due to resonance with the flap modes. Even with the rotor not rotating, the flap and body motions are coupled, with the effect that the flap-pitch and flap-roll frequency pairs move apart. The asymmetry of the body frequencies then produces the split in the regressing

and progressing flap frequencies observed at zero rotor speed.

A calculated mode identified with the inflow dynamics is shown in Fig. 1. More information about the character of this mode is provided by Fig. 6, which shows the locus of the flap and inflow roots as the inflow time lag varies. Only the flap degrees of freedom and the inflow variables were used to calculate these roots. The points shown in Fig. 6 are the quasistatic inflow case ($k = 0$), the case without inflow dynamics ($k = \infty$), and the inflow dynamics model used here ($k = 0.113$). The quasistatic roots are obtained from the roots without inflow dynamics by multiplying the Lock number by the lift deficiency function. The consequence of such a reduction in effective Lock number is a reduction in the damping, with no change in the magnitude of the root (in the rotating frame). In the range $k = 0.00$ to 0.05, the flap motion and inflow variables are highly coupled, as shown by the fact that the regressing flap and inflow modes switch character (also note that the root corresponding to the uncoupled inflow lag for $k = 0.113$ is much different from the coupled inflow roots). As a result of the great coupling with the inflow variables, the regressing flap mode actually has higher damping at $k = 0.113$ than it does without the inflow dynamics; and the inflow mode is a low frequency oscillatory mode, as shown in Fig. 1.

The measured frequencies and regressing lag mode damping are compared with calculations using the quasistatic inflow model in Figs. 7 and 8. The nonrotating body frequencies are still predicted well, but the calculated body frequencies are much too high at rotor speeds above about 300 rpm (Fig. 7). Consequently the resonances with the lag mode are shifted to

higher rotor speeds than in the measurements. In particular the greatest instability at the roll mode resonance is predicted to occur at 900 rpm, instead of 750 rpm as measured (Fig. 8). In addition, the body mode damping is not predicted as well as with the complete inflow dynamics model. Hence for this problem the quasistatic inflow model is not acceptable.

Figs. 9 and 10 show the body mode damping as a function of collective pitch at 650 rpm. Again, the use of the inflow dynamics model produces good correlation, particularly for the roll mode. There is a significant influence of the unsteady aerodynamics even at a collective of 10°, which may be expected since the lift deficiency function is still much less than 1 (Fig. 11). The results with the quasistatic model show a large reduction in damping around a collective pitch of -1.5°, where the thrust is zero and so the static lift deficiency function is also zero.

RESULTS FOR CONFIGURATION 4

In Figs. 12 to 17 the measured modal frequencies and damping for configuration 4 (the stiff flap flexure) are compared with calculations. The collective pitch is zero in this case. Without the inflow dynamics model, the correlation is similar to that for configuration 1: the predicted roll mode frequency is too low at rotor speeds above the resonance (Fig. 13); the regressing lag mode is too stable at the roll mode resonance (Fig. 14); and the calculated roll mode damping is much too high (Fig. 15). In addition, the calculated frequency of the pitch mode does not match either of the modes observed below 3 Hz in the experiment (Fig. 13). The calculated

regressing flap mode has high damping, and so can not correspond to one of the measured modes. The damping of the pitch mode calculated without the inflow dynamics is shown on both Fig. 16 and Fig. 17, but this comparison is not meaningful since the frequency does not match either measured mode. With the inflow dynamics model, the frequencies are well predicted, except for the roll mode at rotor speeds from 250 to 350 rpm (Fig. 12). As for configuration 1, the prediction of the lag mode damping is improved (Fig. 14); and the correlation of the calculated and measured roll mode damping is very good (Fig. 15). Moreover, now two modes are predicted to occur below 3 Hz, and the calculated modes correlate well with the measured modes in both frequency and damping (Figs. 13, 16, and 17). The low frequency mode is now identified as the inflow mode, although its eigenvector involves considerable motion of the body and rotor.

For this configuration, the correlation is not good at the resonance between the regressing flap mode and the body roll mode (Ω = 250 to 350 rpm, Fig. 12). The calculations show much more coupling than the measurements. The frequencies calculated without aerodynamic forces (Fig. 18) show the same effect, so the coupling is due to the structural dynamics of the system. This resonance occurs at a flap frequency of about 1.8/rev, which suggests that the problem involves some high frequency aeroelastic phenomenon. The problem could be a deficiency in the aerodynamic model at high frequencies; or possibly some higher mode of the rotor or body is involved.

The successful prediction of the low frequency modes measured in the test of configuration 4 raises further questions. First, what is this

inflow mode? That is is measureable is surprising, since in fact the inflow variables λ_x and λ_y do not correspond to real physical states of the system. This mode may be interpreted as follows. The unsteady aerodynamics introduces behavior of the system, as observed in either the time or frequency domain, that can be approximated by an additional oscillatory mode with low or moderate damping (the experimental procedure used to measure the frequency and damping only works for such modes). Approximating the behavior by an additional mode implies then the existence of additional states or degrees of freedom of the system.

The second question is why the inflow mode was observed in the tests of configuration 4, but not for configuration 1. With increased flap stiffness, the regressing flap mode will be more coupled with the body motion. The great coupling between the flap motion and inflow variables then implies that the inflow dynamics will have more influence on the body motions for configuration 4 than for configuration 1. The pitch and inflow modes were measured by applying a pitch moment impulse to the body. Then the modal frequencies were identified from the magnitude of the spectrum of the resulting transient pitch motion; and the corresponding damping was estimated using the moving block technique (Ref. 1). Consider what the calculations imply about the task of identifying the pitch and inflow modes from the body pitch motion. Figs. 19 and 20 show the damping ratio of the low frequency modes for the two configurations, and Table 3 summarizes the results for Ω = 650 rpm. For configuration 4 relative to configuration 1,

Table 3. Body Pitch and Inflow Mode Characteristics (Ω = 650 rpm)

	Configuration 1	Configuration 4
Pitch mode		
Frequency	1.84 Hz	2.0? Hz
Damping ratio	0.11	0.1?
Inflow mode		
Frequency	0.43 Hz	0.74 Hz
Damping ratio	0.59	0.37
Ratio contributions of inflow and pitch modes to pitch motion	0.0?	0.2?

the damping ratio of the pitch mode is increased while the damping ratio of the inflow mode is decreased. This implies that the inflow mode will be more observable for configuration 4, since the damping ratio determines the relative width of the resonant peaks. Note that with a damping ratio of 0.6, the frequency response will hardly show a resonant peak at all. In addition, the small frequency of the inflow mode for configuration 1 would make it more difficult to measure that mode, since the experimental data reduction procedure had a frequency resolution of 0.2 Hz. The response of the body pitch motion to an applied moment can be characterized by a pole-zero plot, shown in Figs. 21 and 22 for the two configurations. The larger separation of the inflow root from the zero for configuration 4 implies more participation of the inflow mode in the pitch response. The modal contribution can be quantified by considering the ratio of the coefficients of the pitch and inflow modes in the partial fraction expansion of the pitch response. This ratio is 9% for configuration 1, and 30% for configuration 4 (Table 3; the next largest contributions, from the regressing flap and lag modes, are approximately 10% of the contribution of the inflow mode). The frequency response of the body pitch motion to an applied moment is shown in Figs. 23 and 24 for the two configurations. The calculations confirm that the inflow mode should be observable for configuration 4, but not for configuration 1.

CONCLUSIONS

Calculations of the modal frequencies and damping for a hingeless rotor on a gimballed support in hover have shown good correlation with

measurements when an inflow dynamics model is used to account for the influence of unsteady aerodynamics. The influence of the unsteady aerodynamics was significant for this system. One of the modes in the measured data has been identified as an inflow mode, demonstrating that the unsteady aerodynamics are well represented by an augmented state model in this case, and that the inflow dynamics mode is directly measureable. The remaining discrepancy between the measured and calculated results involved the resonance between the flap and roll modes at low rotor speed for configuration 4. Further development and verification of this inflow dynamics model will require comparison with data for additional rotor systems, and extension of these investigations to forward flight.

REFERENCES

1 Bousman, W.G., "An Experimental Investigation of the Effects of Aeroelastic Couplings on Aeromechanical Stability of a Hingeless Rotor Helicopter." Journal of the American Helicopter Society, 26, 1, January 1981.

2 Johnson, W., Helicopter Theory. Princeton University Press, Princeton, New Jersey, 1980.

3 Johnson, W., "A Comprehensive Analytical Model of Rotorcraft Aerodynamics and Dynamics." NASA TM 81182, June 1980.

4 Miller, R.H., "Rotor Blade Harmonic Air Loading." AIAA Journal, 2, 7, July 1964.

5 Pitt, D.M., and Peters, D.A., "Theoretical Prediction of Dynamic Inflow Derivatives." European Rotorcraft and Powered Lift Aircraft Forum, Bristol, England, September 1980.

6 Crews, S.T.; Hohenemser, K.H.; and Ormiston, R.A., "An Unsteady Wake Model for a Hingeless Rotor." Journal of Aircraft, 10, 12, December 1973.

7 Banerjee, D.; Crews, S.T.; Hohenemser, K.H.; and Yin, S.K., "Identification of State Variables and Dynamic Inflow from Rotor Model Dynamic Tests." Journal of the American Helicopter Society, 22, 2, April 1977.

8 Peters, D.A., "Hingeless Rotor Frequency Response with Unsteady Inflow." NASA SP-352, February 1974.

9 Carpenter, P.J., and Fridovich, B., "Effect of a Rapid Blade-Pitch Increase on the Thrust and Induced-Velocity Response of a Full-Scale Helicopter Rotor." NACA TN 3044, November 1953.

10 Rebont, J.; Valensi, J.; and Soulez-Lariviere, J., "Response of a Helicopter Rotor to an Increase in Collective Pitch for the Case of Vertical Flight." NASA TT F-55, January 1961.

11 Curtiss, H.C., Jr., and Shupe, N.K., "A Stability and Control Theory for Hingeless Rotors." Annual National Forum of the American Helicopter Society, Washington, D.C., May 1971.

12 Ormiston, R.A., and Peters, D.A., "Hingeless Helicopter Rotor Response with Nonuniform Inflow and Elastic Blade Bending." Journal of Aircraft, 9, 10, October 1972.

13 Seckel, E., Stability and Control of Airplanes and Helicopters. Academic Press, New York, 1964.

14 Gaonkar, G.H., and Peters, D.A., "Use of Multiblade Coordinates for Helicopter Flap-Lag Stability with Dynamic Inflow." Journal of Aircraft, 17, 2, February 1980.

15 Peters, D.A., and Gaonkar, G.H., "Theoretical Flap-Lag Damping with Various Dynamic Inflow Models." Journal of the American Helicopter Society, 25, 3, July 1980.

16 Banerjee, D.; Crews, S.T.; and Hohenemser, K.H., "Parameter Identification Applied to Analytic Hingeless Rotor Modelling." Journal of the American Helicopter Society, 24, 1, January 1979.

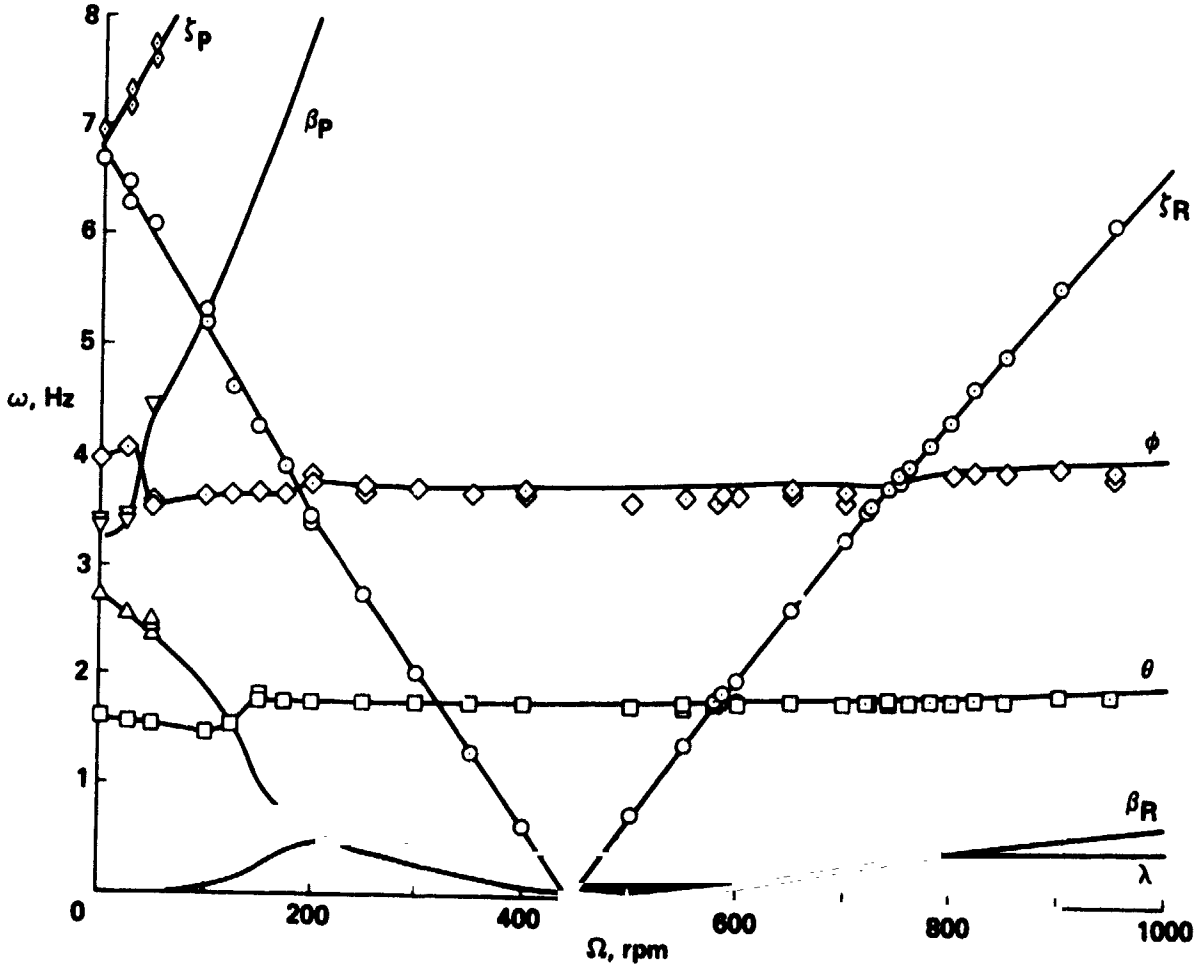

Figure 1. Modal frequencies as a function of rotor speed for configuration 1: comparison of measurements (points) and calculations including inflow dynamics (lines).

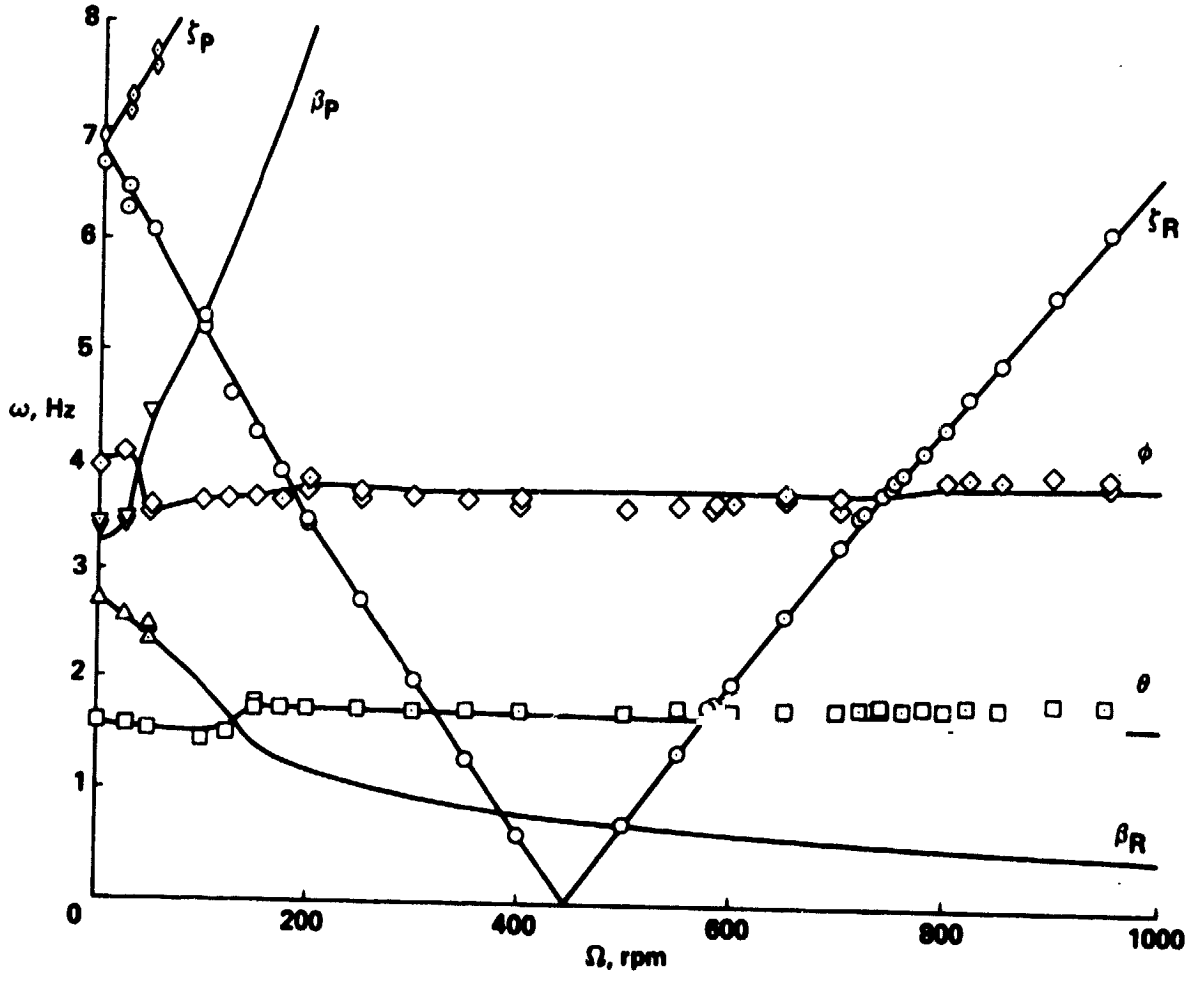

Figure 7. Modal frequencies as a function of rotor speed for configuration 1: comparison of measurements (points) and calculations without inflow dynamics (lines).

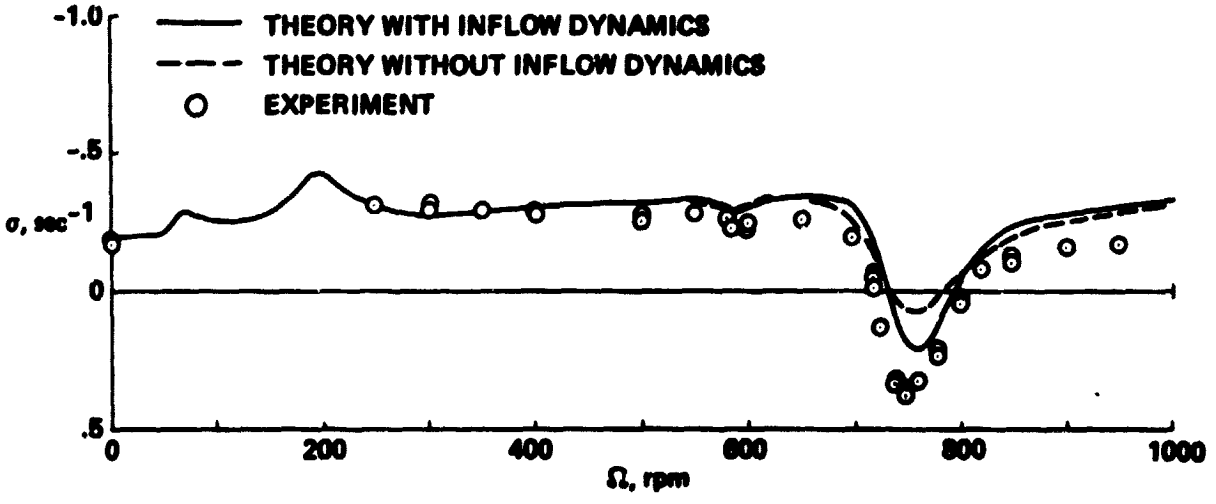

Figure 3. Regressing lag mode damping as a function of rotor speed for configuration 1.

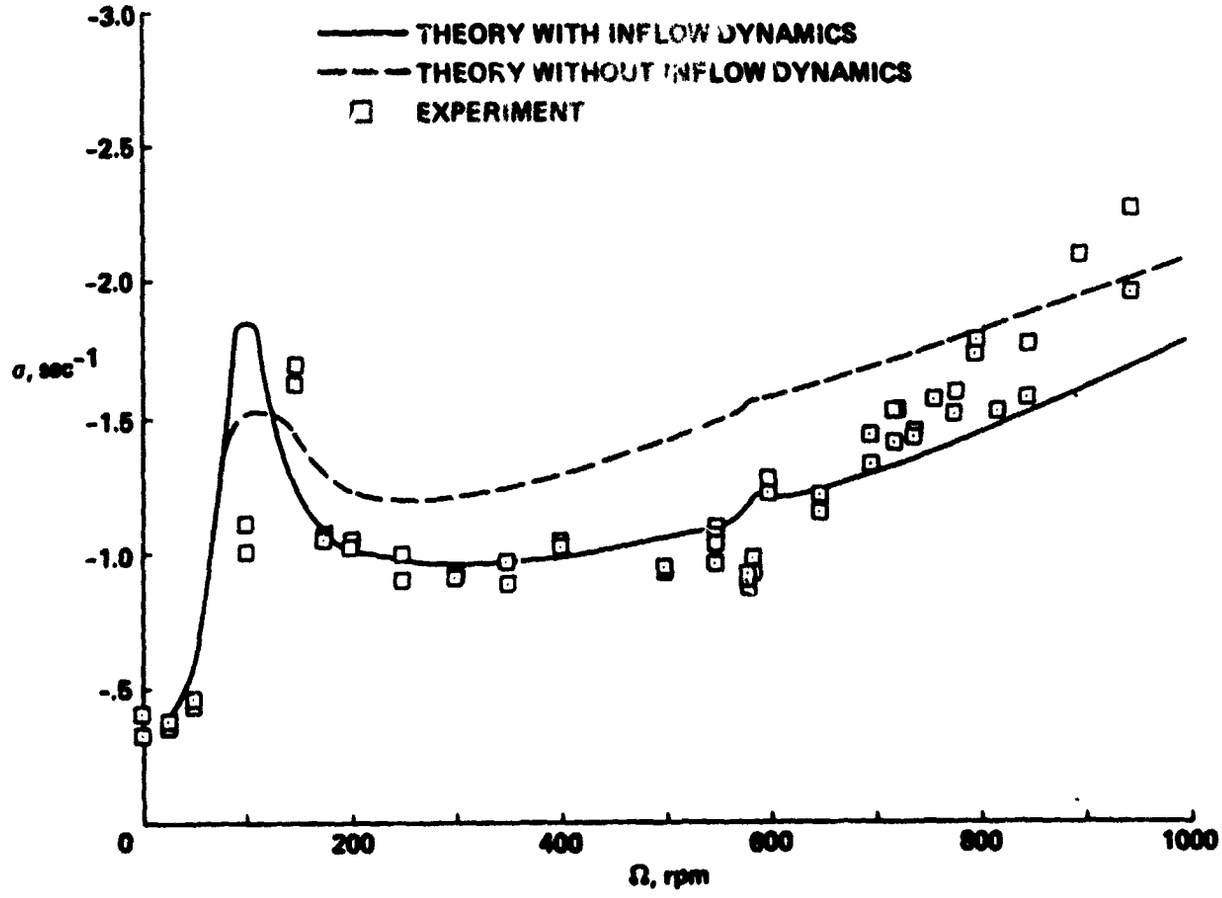

Figure 4. Body pitch mode damping as a function of rotor speed for configuration 1.

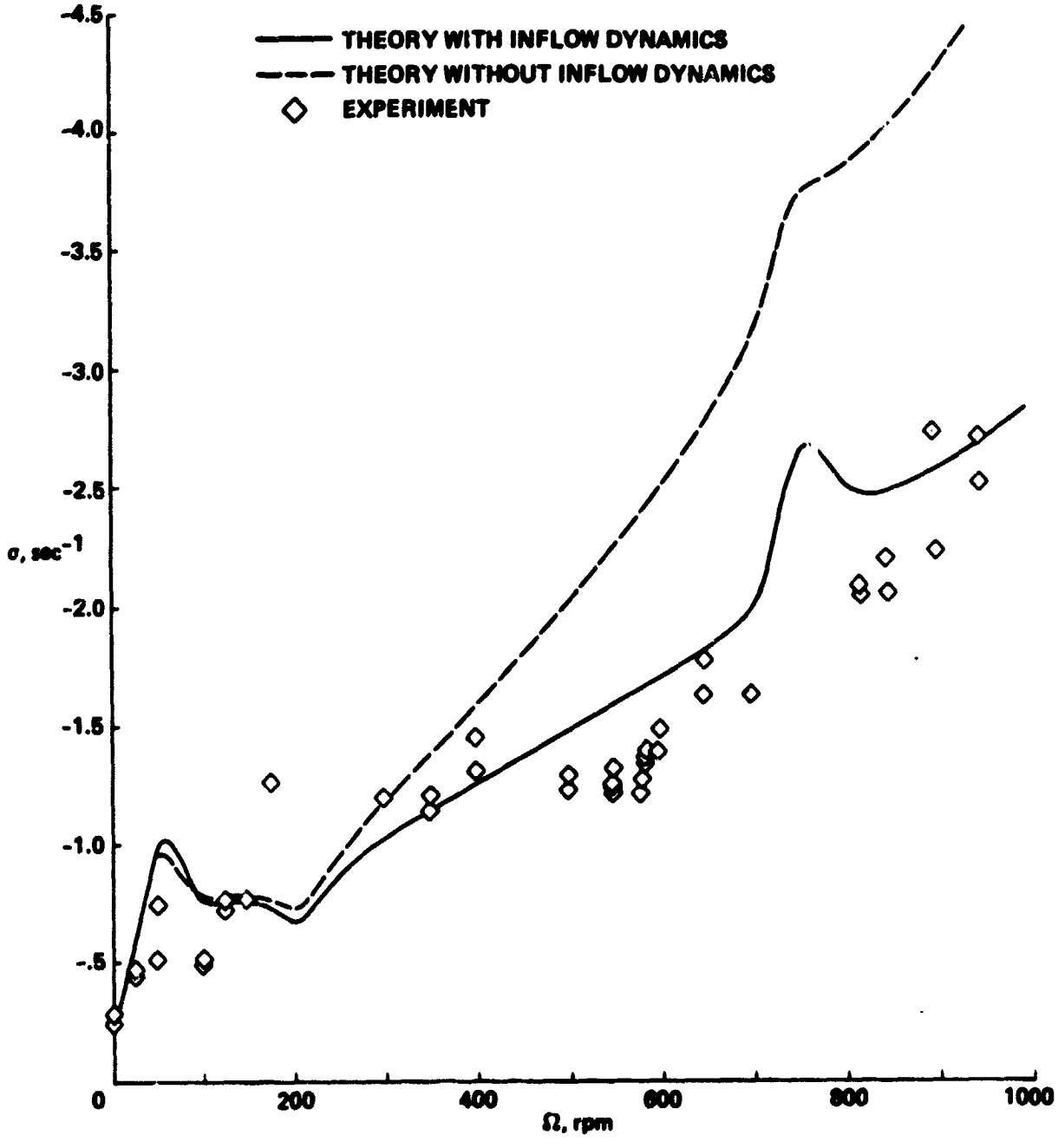

Figure 5. Body roll mode damping as a function of rotor speed for configuration 1.

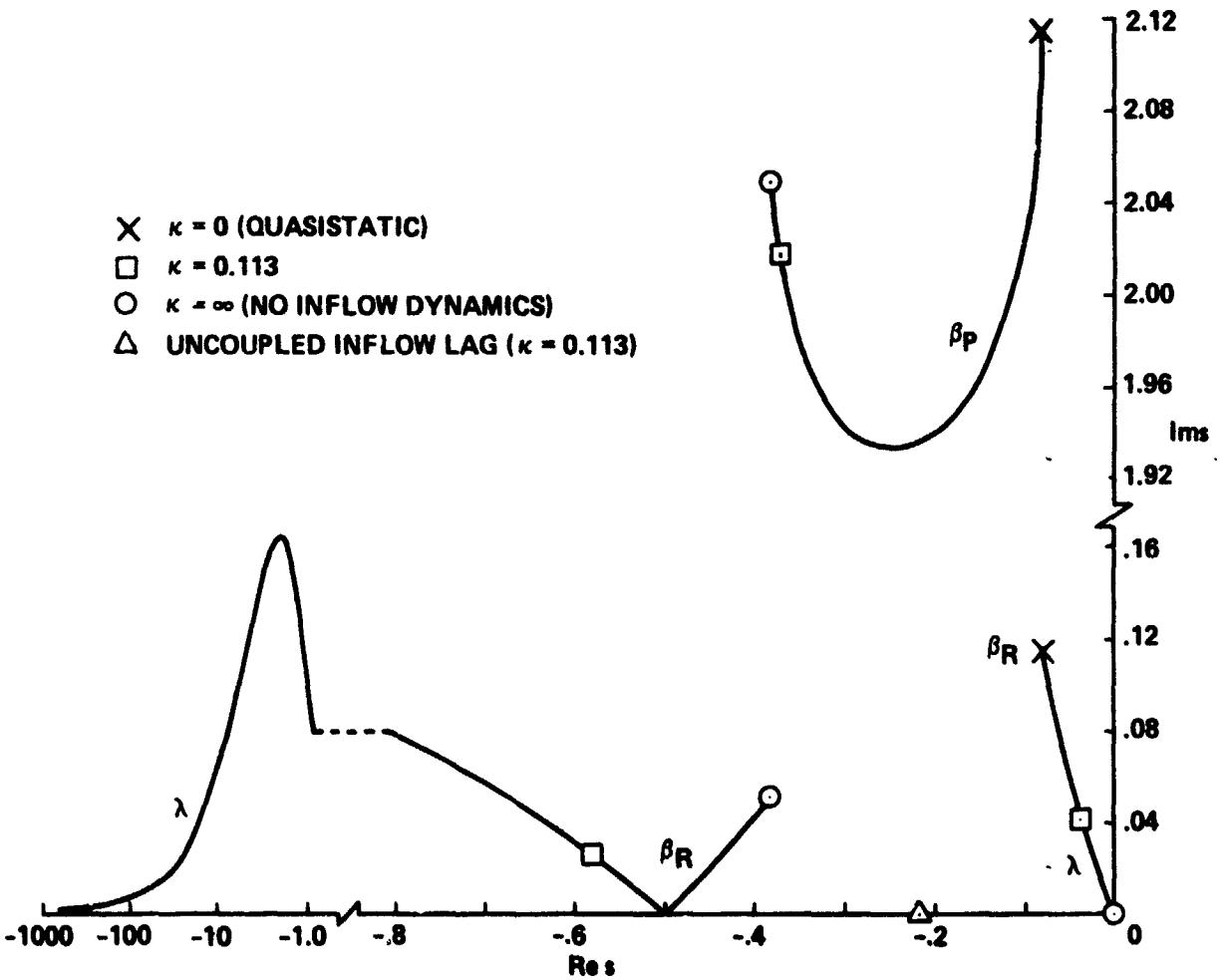

Figure 6. Root locus showing influence of inflow time lag on coupled dynamics of blade flap and inflow degrees of freedom (Ω = 650 rpm, configuration 1; dimensionless scales).

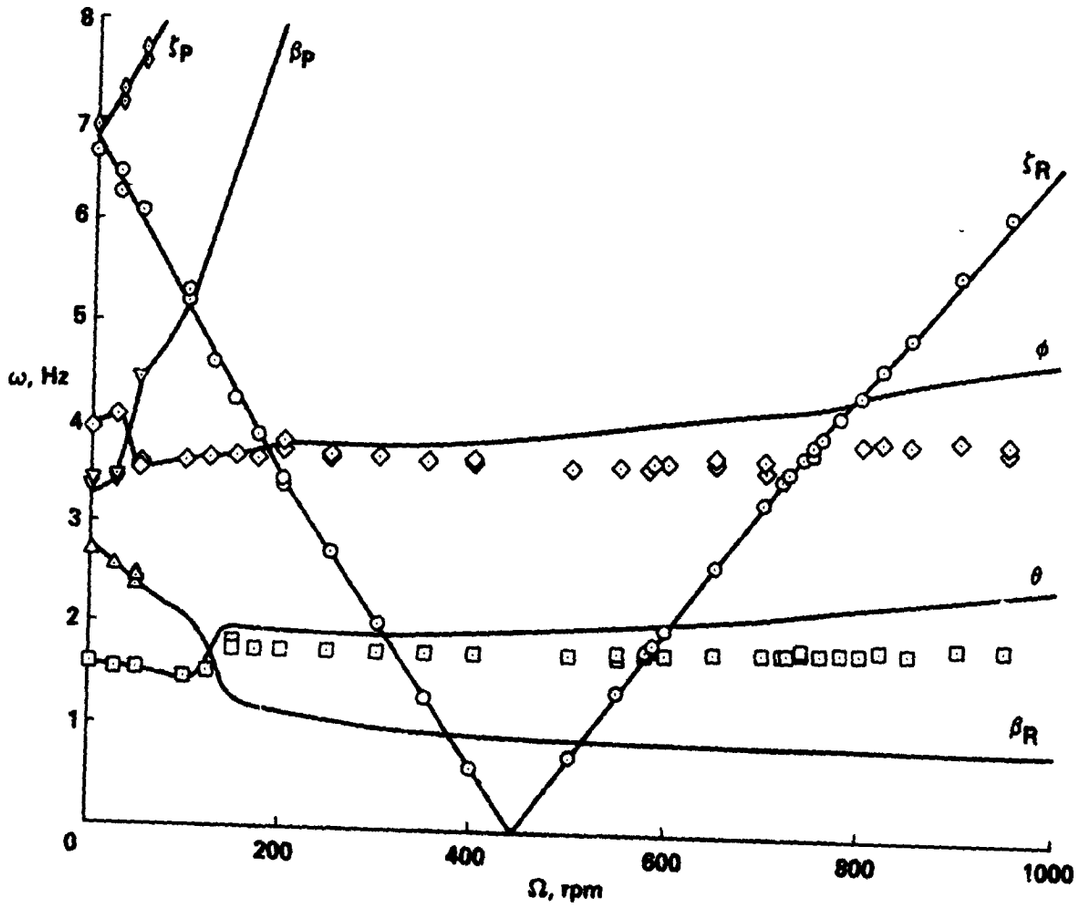

Figure 7. Modal frequencies as a function of rotor speed for configuration 1: comparison of measurements (points) and calculations with quasistatic inflow model (lines).

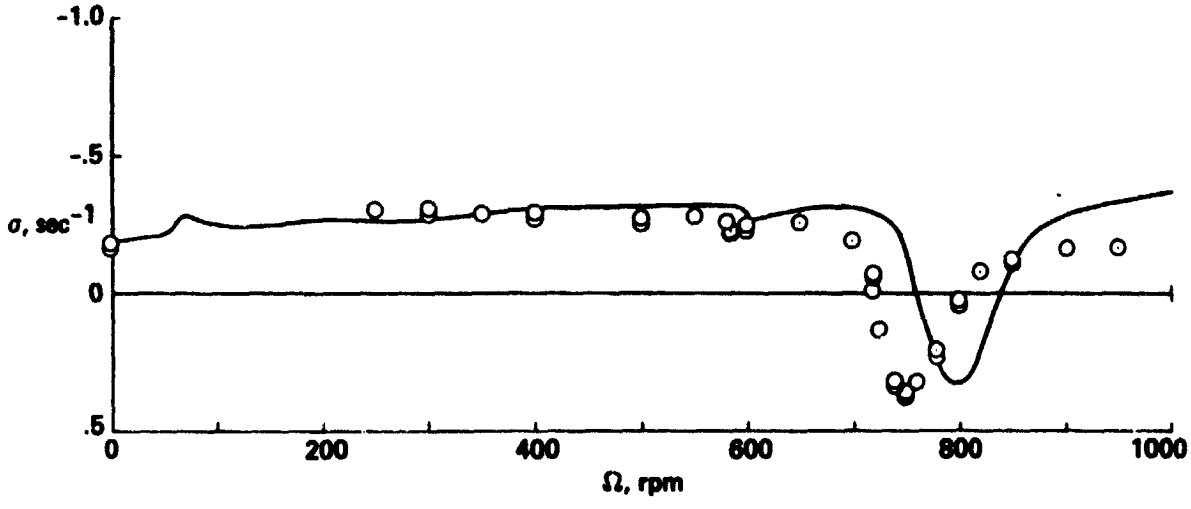

Figure 8. Regressing lag mode damping as a function of rotor speed for configuration 1: comparison of measurements (points) and calculations with quasistatic inflow model (lines).

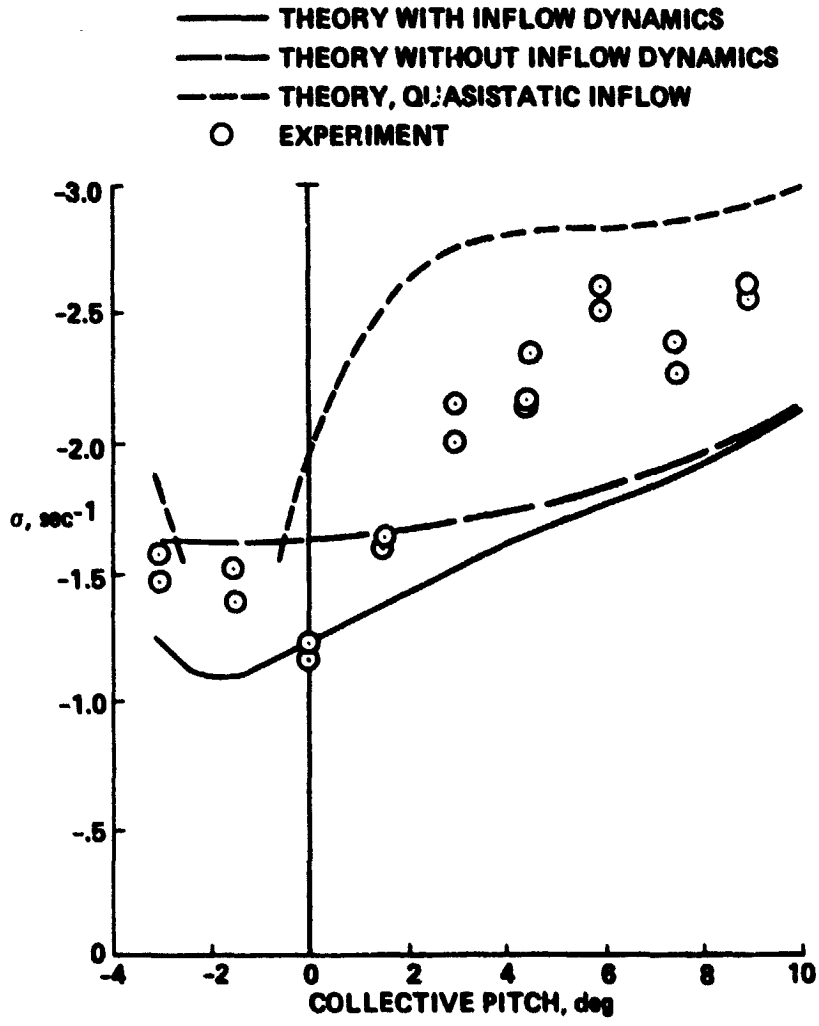

Figure 9. Body pitch mode damping as a function of collective pitch for configuration 1 (Ω = 650 rpm).

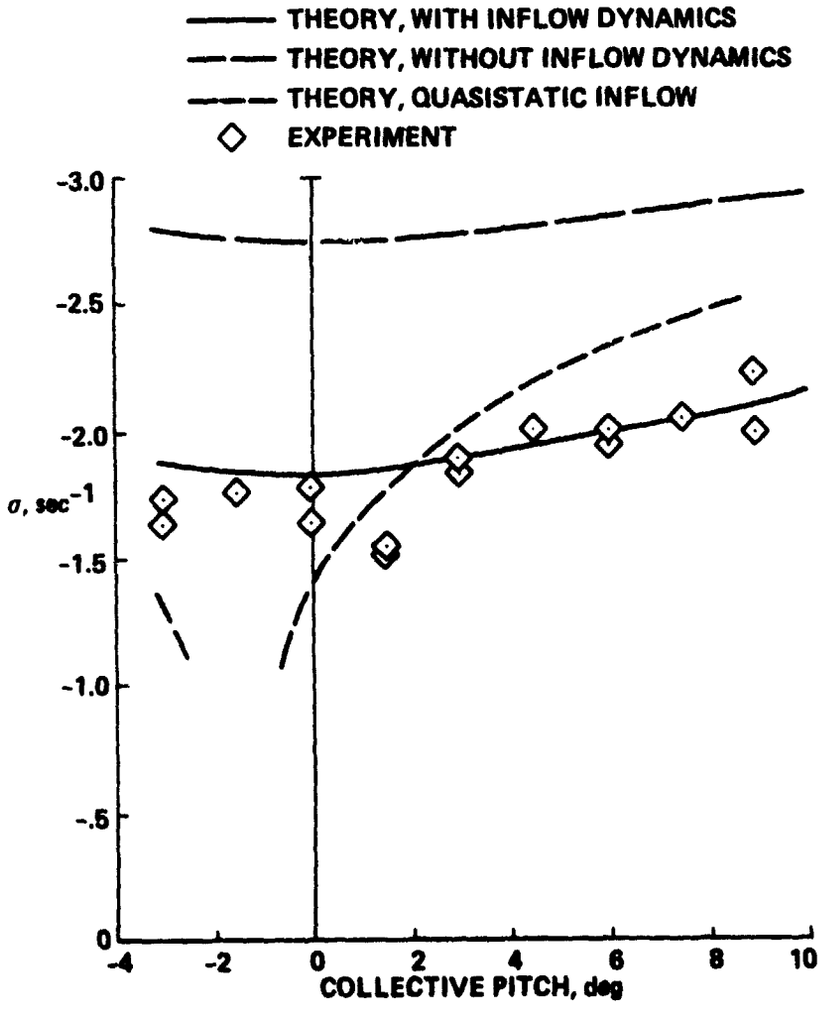

Figure 10. Body roll mode damping as a function of collective pitch for configuration 1 (Ω = 650 rpm).

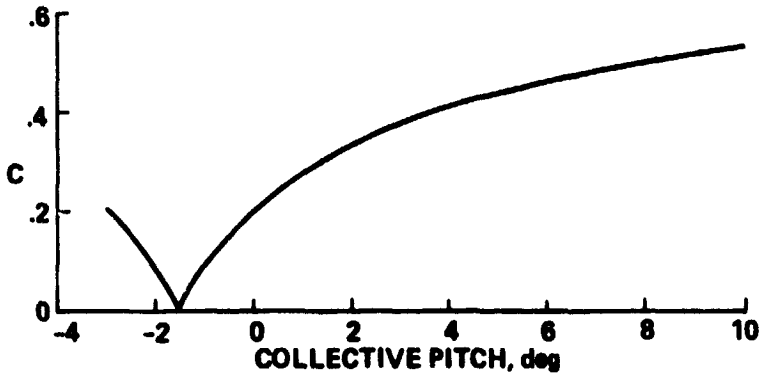

Figure 11. Lift deficiency function variation with collective pitch.

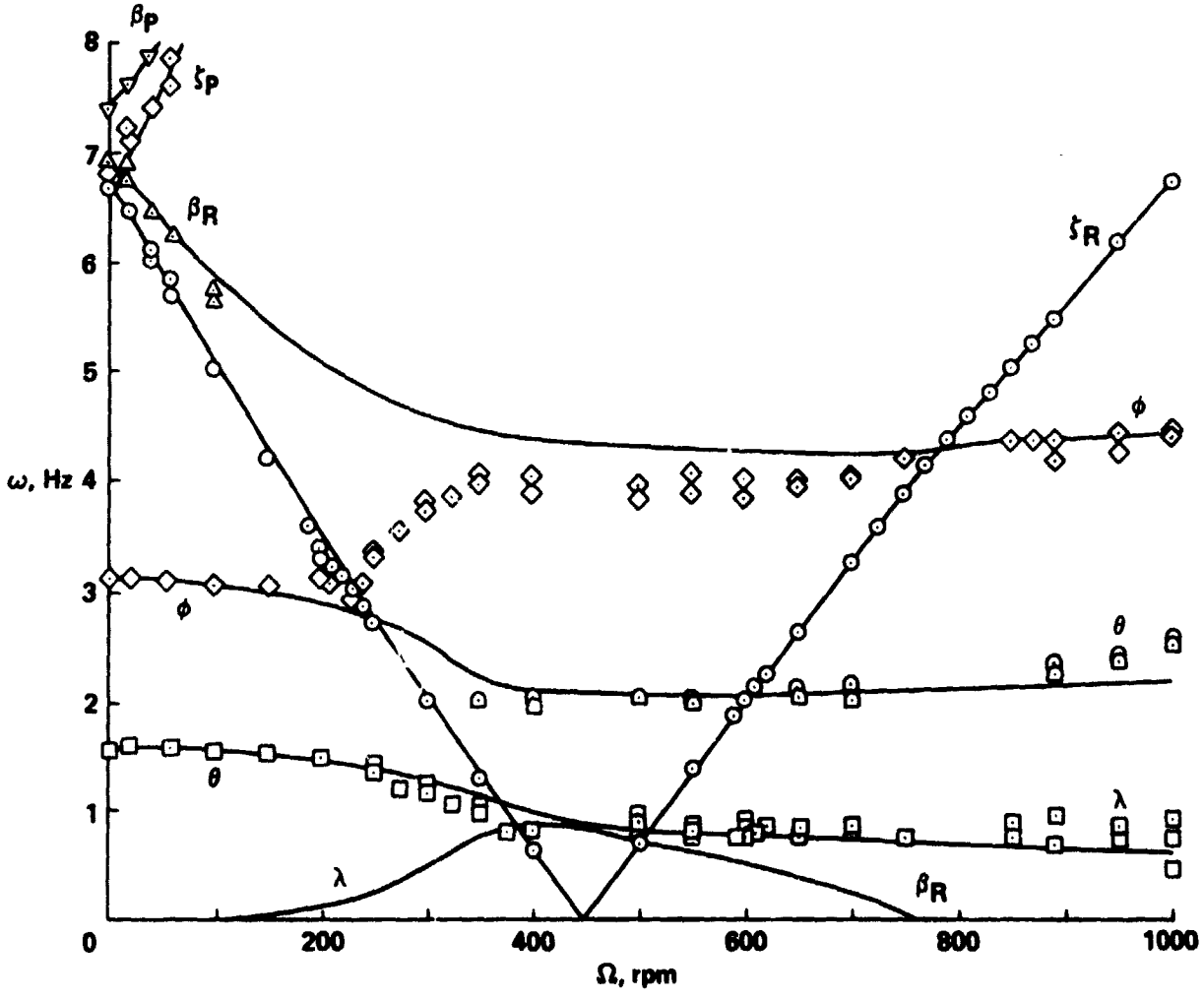

Figure 17. Modal frequencies as a function of rotor speed for configuration 4: comparison of measurements (points) and calculations including inflow dynamics (lines).

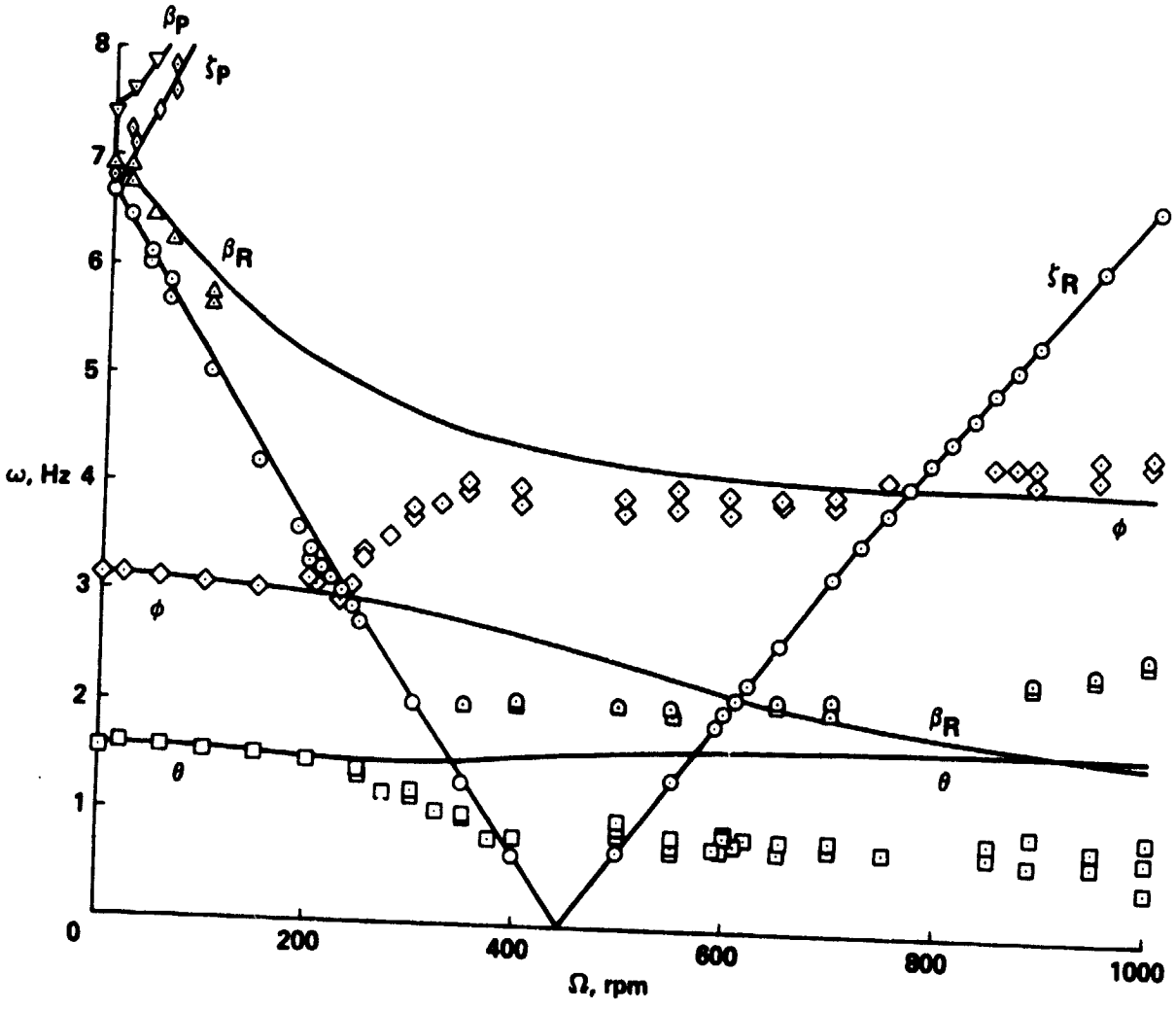

Figure 13. Modal frequencies as a function of rotor speed for configuration A; comparison of measurements (points) and calculations without inflow dynamics (lines).

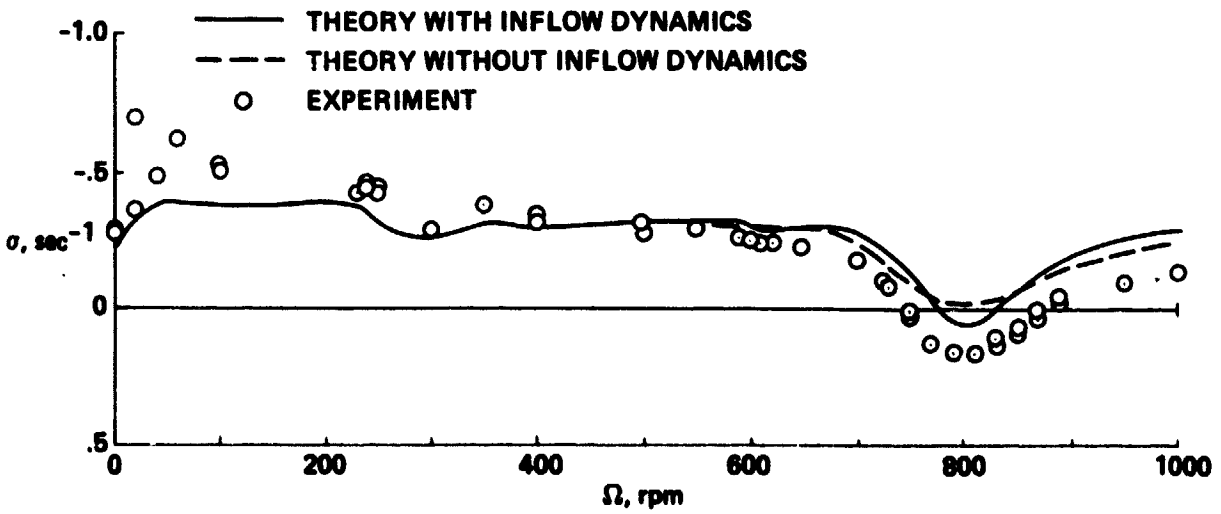

Figure 14. Regressing lag mode damping as a function of rotor speed for configuration 4.

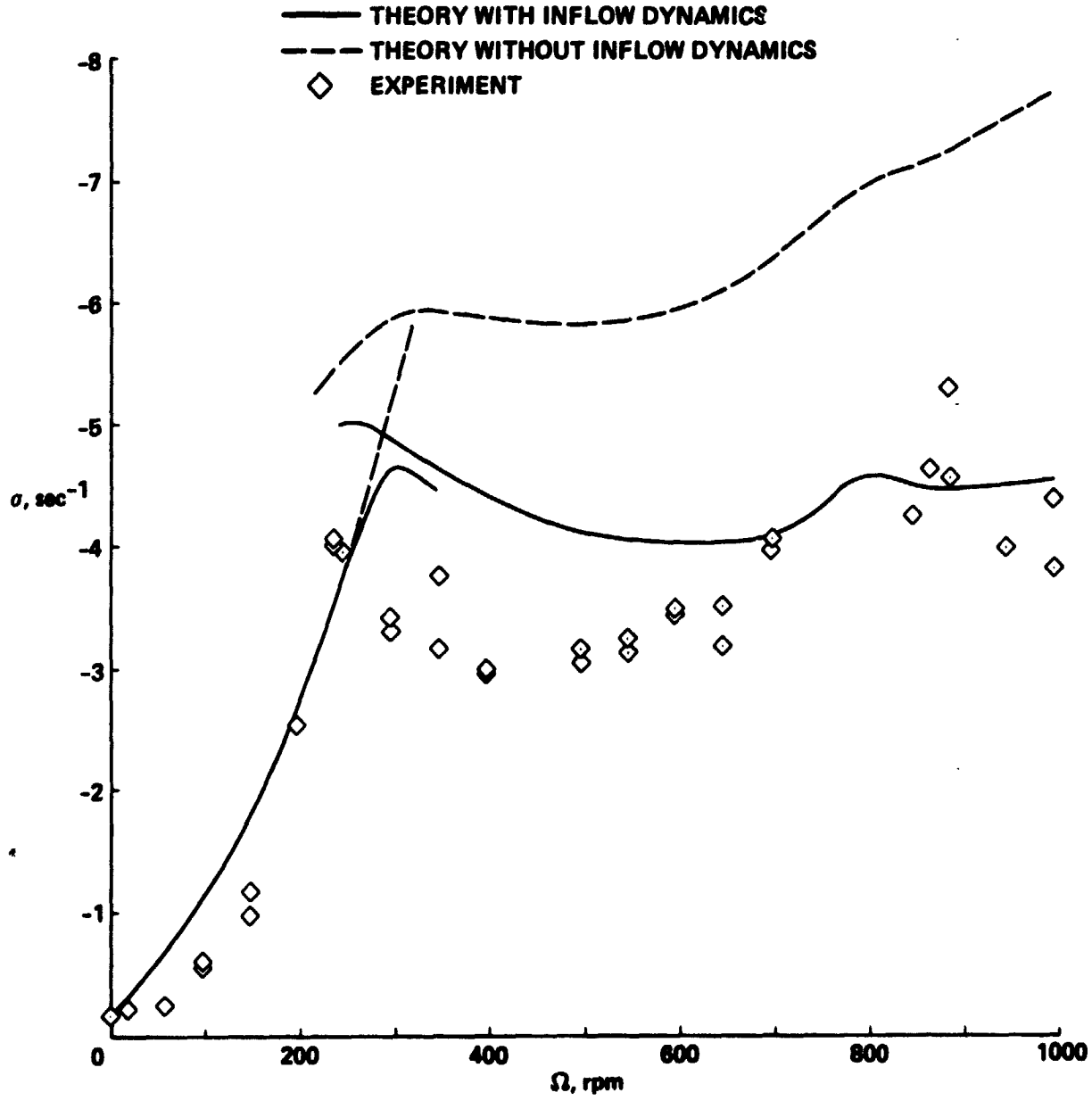

Figure 15. Body roll mode damping as a function of rotor speed for configuration 4.

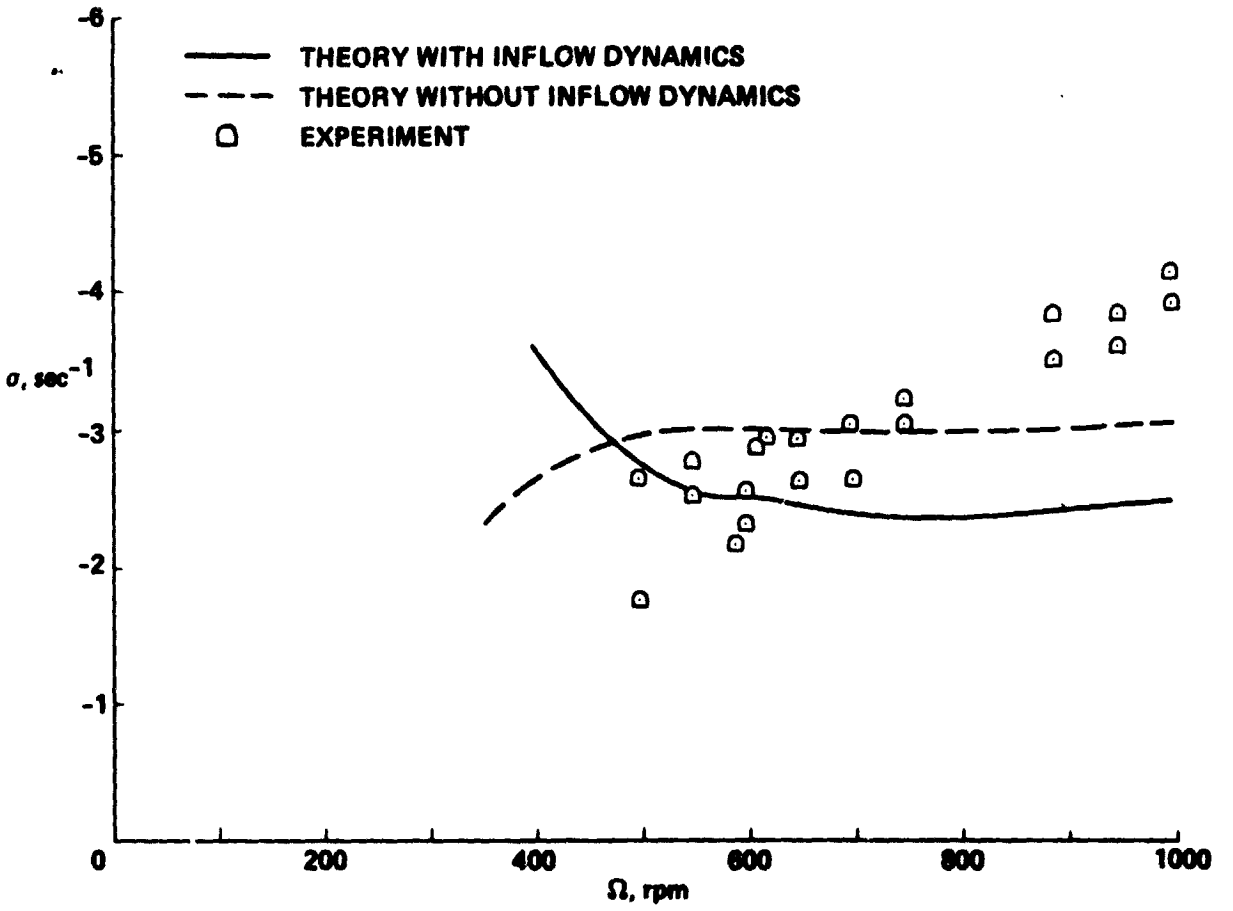

Figure 16. Body pitch mode damping as a function of rotor speed for configuration 4.

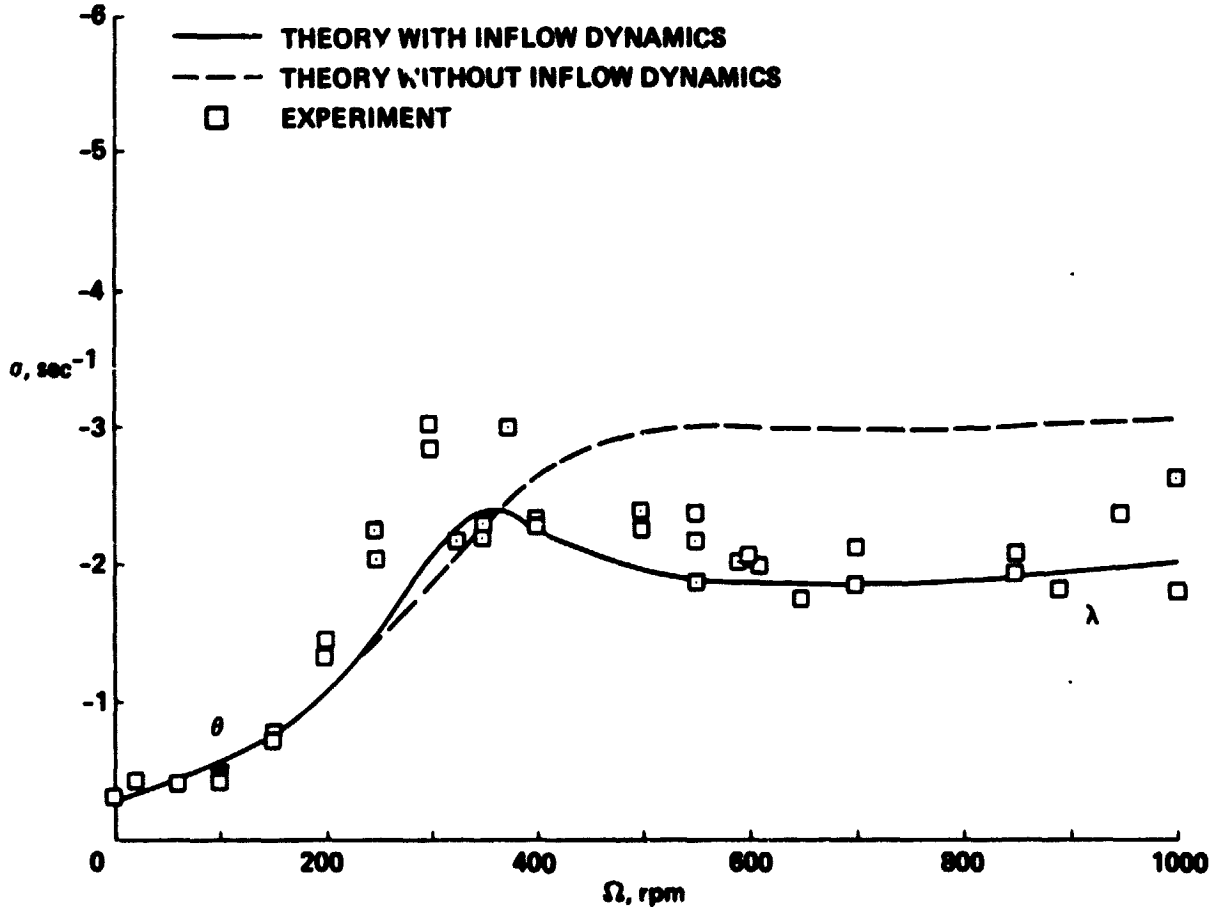

Figure 17. Body inflow and pitch mode damping as a function of rotor speed for configuration A.

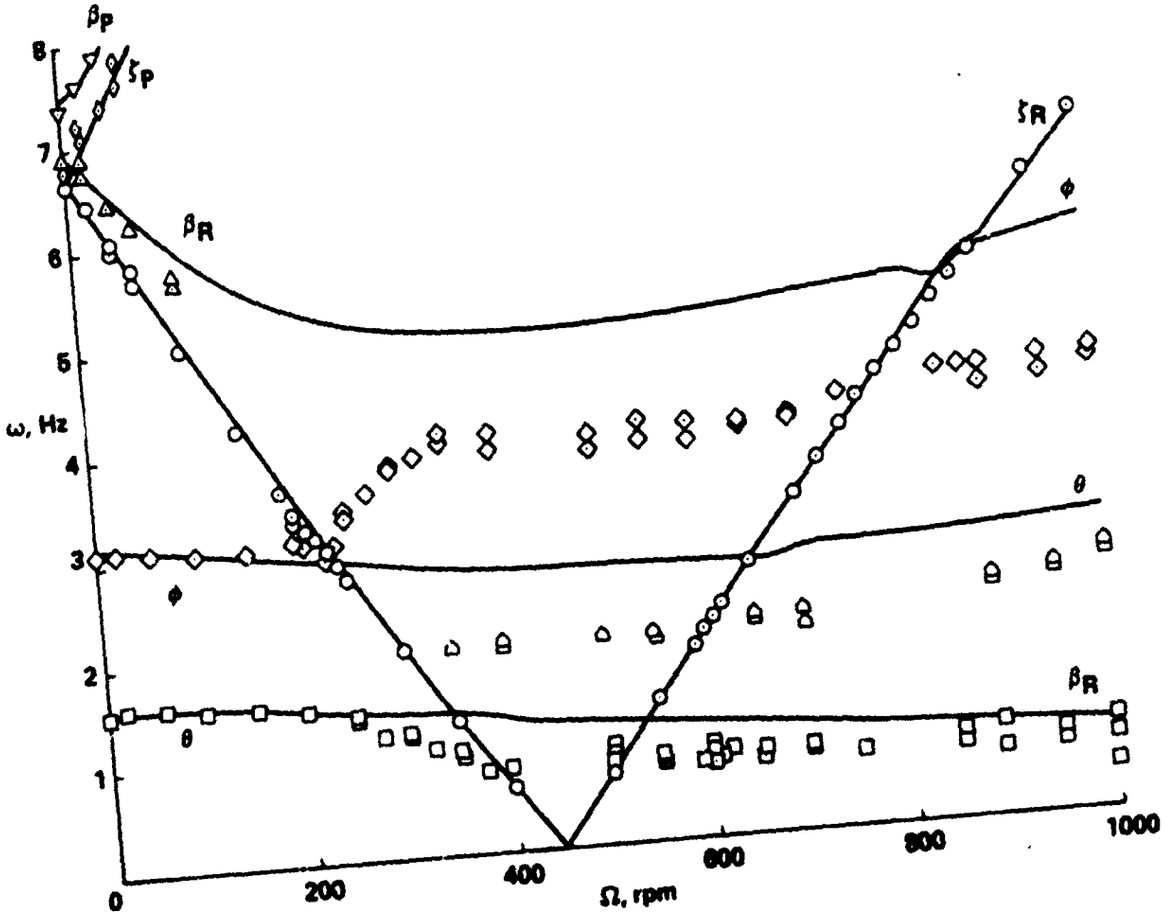

Figure 18. Modal frequencies as a function of rotor speed for configuration A; comparison of measurements (points) and calculations without aerodynamics (lines).

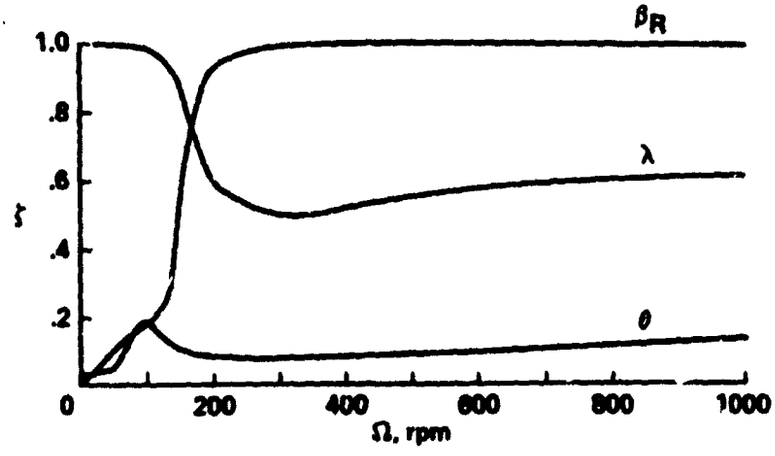

Figure 19. Calculated modal damping ratio as a function of rotor speed for configuration 1.

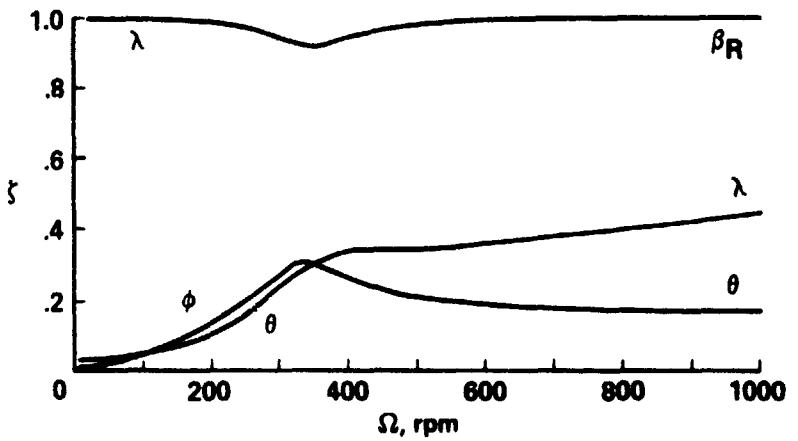

Figure 20. Calculated modal damping ratio as a function of rotor speed for configuration 4.

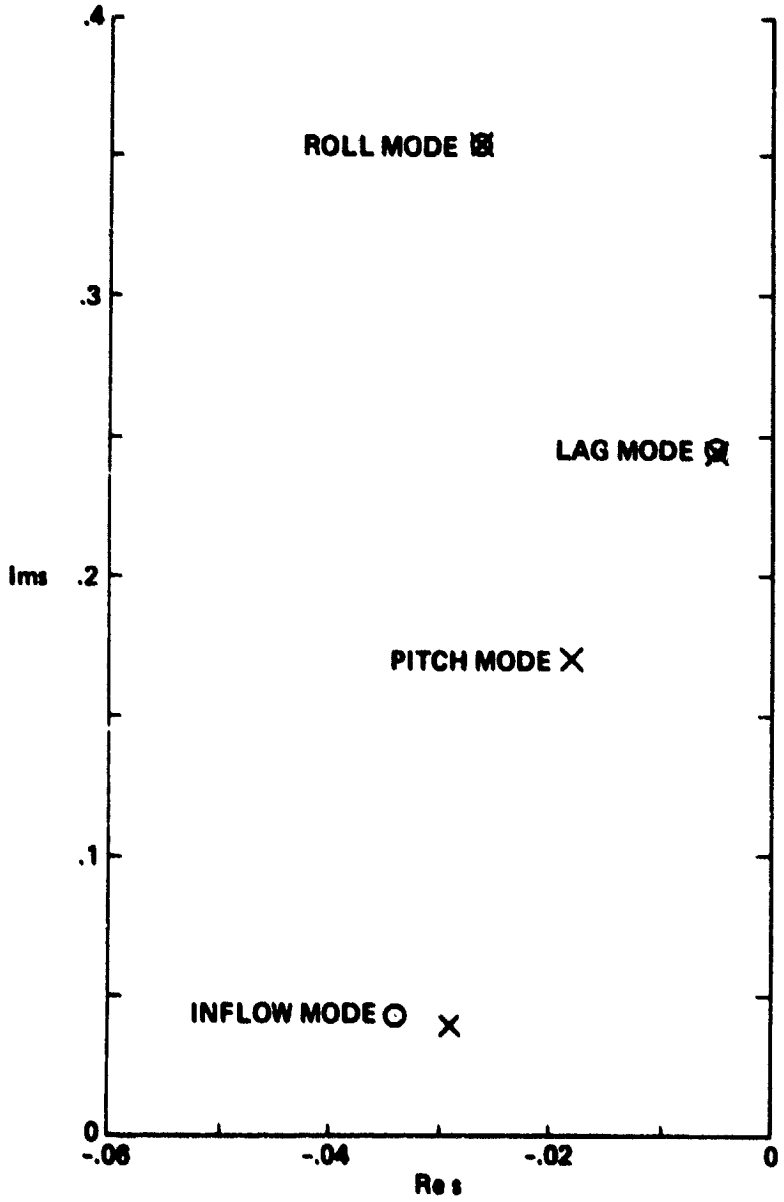

Figure 21. Calculated poles (x) and zeros (o) of body pitch motion response to an applied moment for configuration 1 (450 rpm; dimensionless scales).

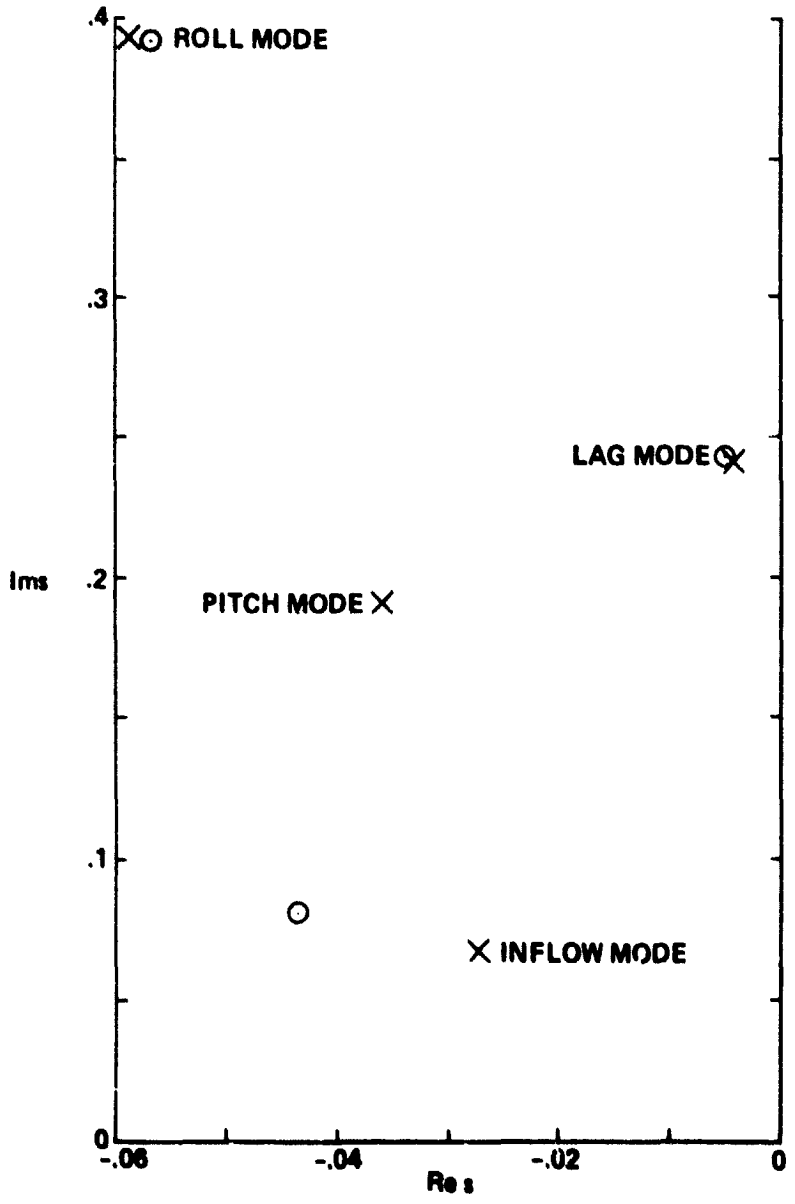

Figure 22. Calculated poles (x) and zeros (o) of body pitch motion response to an applied moment for configuration B (650 rpm; dimensionless scales).

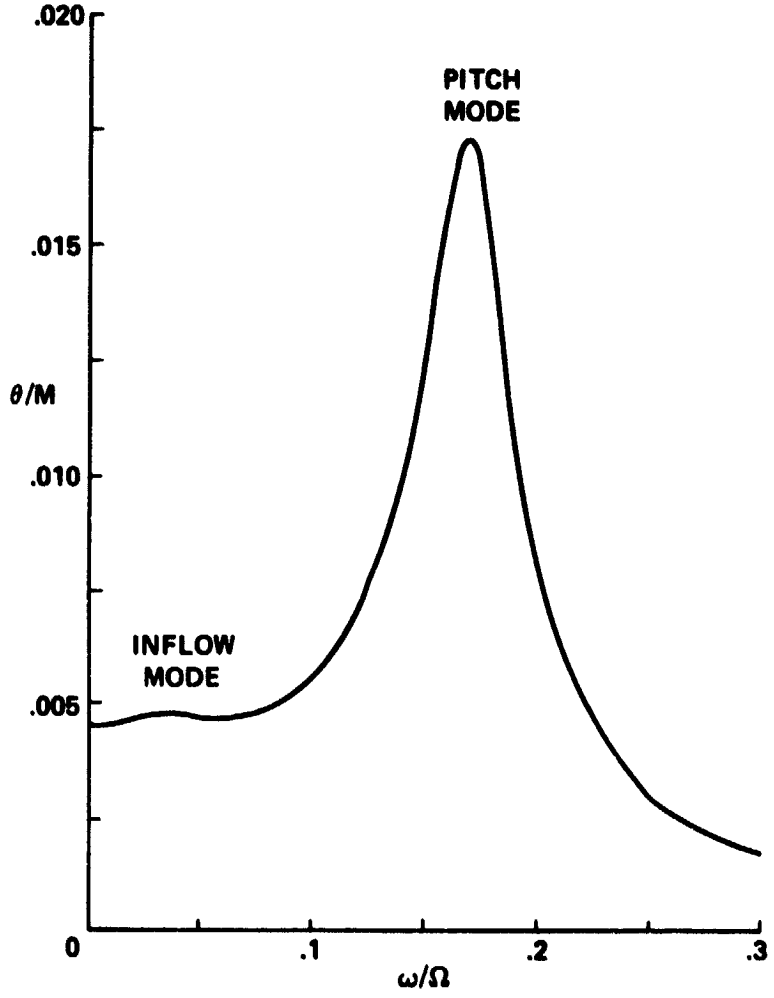

Figure 23. Magnitude of the calculated frequency response of the body pitch motion to an applied moment for configuration 1 (650 rpm; dimensionless scales).

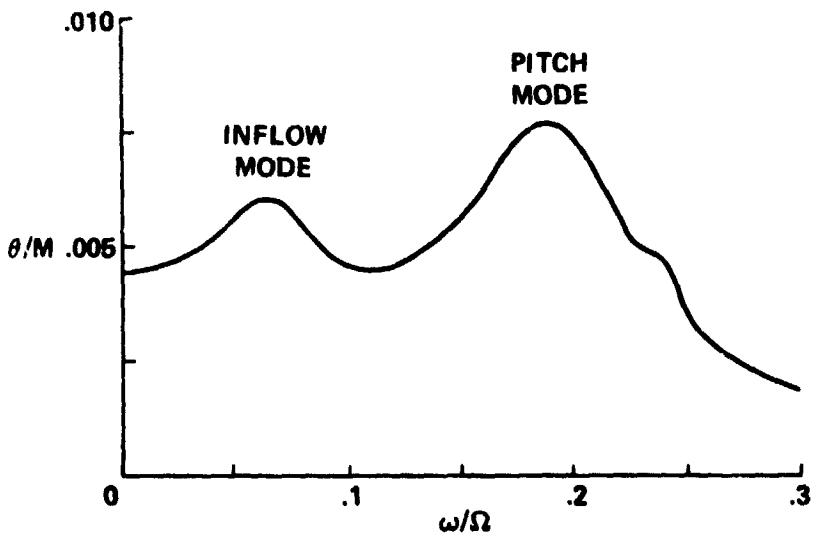

Figure 24. Magnitude of the calculated frequency response of the body pitch motion to an applied moment for configuration b (650 rpm; dimensionless scales).